Available online at www.sciencedirect.com

ScienceDirect

Proceedings of the Combustion Institute 36 (2017) 1165–1173

Proceedings of the Combustion Institute

www.elsevier.com/locate/proci

Experimental and kinetic modeling study of diethyl ether flames

Luc-Sy Tran [a,*], Julia Pieper [a], Hans-Heinrich Carstensen [b], Hao Zhao [c], Isabelle Graf [a], Yiguang Ju [c], Fei Qi [d], Katharina Kohse-Höinghaus [a]

[a] *Department of Chemistry, Bielefeld University, Universitätsstraße 25, D-33615 Bielefeld, Germany*
[b] *Laboratory for Chemical Technology (LCT), Ghent University, Technologiepark 914, 9052 Ghent, Belgium*
[c] *Department of Mechanical and Aerospace Engineering, Princeton University, Princeton NJ 08544, USA*
[d] *Key Laboratory for Power Machinery and Engineering of MOE, Shanghai Jiao Tong University, Shanghai 200240, PR China*

Received 25 November 2015; accepted 10 June 2016
Available online 24 June 2016

Abstract

Diethyl ether (DEE, $C_4H_{10}O$) is being considered as a promising biofuel. However, its combustion chemistry has not been well studied. Particularly lacking are quantitative intermediate species profiles in flames that provide a stringent test for kinetic models, and flame speed data at elevated pressures. In the present paper, we obtain species distributions in low-pressure flames and measure flame speeds at elevated pressure to gain insights into high-temperature combustion chemistry of DEE. Specifically, a fuel-rich DEE flame ($\phi \sim 1.8$) with 25% argon dilution at 4 kPa was investigated by using a dedicated combination of electron ionization (EI) molecular-beam mass spectrometry (MBMS) with gas chromatography (GC) and tunable synchrotron vacuum ultraviolet (VUV) photoionization (PI) MBMS. High-pressure flame speeds of DEE were measured in a constant-volume cylindrical chamber at an initial temperature of 298 K at an equivalence ratio of $\phi = 1.4$ and pressure up to 507 kPa. Moreover, a new detailed kinetic model for DEE combustion was developed, with the most noticeable advances over the solely existing model by Yasunaga et al., 2010 being a more complete description of the reactions of DEE radicals and the use of accurate theoretical methods, *i.e.* CBS-QB3, to determine the rate constants for important primary reactions. In contrast to the previously published one, the present model includes reactions of DEE radicals that directly involve the formation of ethyl vinyl ether (EVE), an addition supported by identification and quantification of EVE by PI-MBMS in the flame experiment. Finally, the results showed that DEE flames yield low concentrations of aromatic species. However, high acetaldehyde emission was observed, originating from the dominant pathways of DEE consumption via H-abstractions from C_{α} positions followed by β-scissions.

Keywords: Biofuel; Diethyl ether; Laminar premixed flame; Molecular-beam mass spectrometry; Detailed kinetic model

1. Introduction

Increasing energy demand in the transport sector, coupled with the need to reduce greenhouse gas

* Corresponding author.
E-mail addresses: luc-sy.tran@uni-bielefeld.de, tran.luc.sy.iutdn@gmail.com (L.-S. Tran).

http://dx.doi.org/10.1016/j.proci.2016.06.087
1540-7489

emissions, continues to motivate research directed toward renewable fuels. Biofuels such as ethers, esters, and alcohols are discussed as additives or replacement fuels [1]. Diethyl ether (DEE), available via dehydration of ethanol over solid acid catalysts, is considered as a promising biofuel [2,3]. DEE has several favorable properties for diesel engine combustion including a high cetane number (>125) and energy density (33.9 MJ/kg), more favorable than that of dimethyl ether (28.6 MJ/kg), broad flammability limits, and high miscibility with diesel fuel [3]. Unfortunately, only limited investigations on the combustion chemistry of DEE have been performed, including measurements of ignition delay times [4,5], species profiles from pyrolysis and a non-premixed flame [5,6], and flame speeds [7–9]. Data are particularly scarce regarding species profiles in DEE combustion. Especially intermediate species profiles in laminar flames are known to provide a stringent test for kinetic models that may then be used for the prediction of pollutant emissions. To the best of our knowledge, quantitative sets of species profiles in premixed DEE flames are not yet available. We have thus studied the combustion chemistry of DEE in a fuel-rich low-pressure laminar premixed flame by investigating a full set of species profiles with a combination of advanced analytic techniques. To broaden the available parameter range, we also measured the laminar flame speeds of DEE in a constant-volume chamber at elevated pressure. A new detailed kinetic model relying on a systematic analysis of DEE radical reactions is proposed to describe the combustion of DEE, in particular with respect to intermediates and pollutant formation.

2. Experiments and Modeling

2.1. Flame experiments

A fuel-rich ($\phi \sim 1.8$, C/O ~ 0.52) premixed flame of DEE/oxygen/argon (17.3%/57.7%/25%) was stabilized on a home-made flat burner (McKenna type) of 64 mm diameter (Bielefeld) at 4 kPa, with a cold gas velocity (333 K, 4 kPa) of 73 cm/s and an overall mass flow rate of 4.35×10^{-3} g/(cm^2 s). Adapted conditions to provide the same mass flow rate were applied with a McKenna burner of 60 mm diameter at the Taiwan Light Source. An EI-MBMS-GC setup (Bielefeld) was used, complemented with a VUV-PI-MBMS system (Taiwan), to provide a detailed chemical analysis of stable and reactive species together with isomer identification.

2.2. EI-MBMS-GC experiment

A detailed description of the experimental setup is given elsewhere [10]. In brief, gas samples were extracted from the flame by a quartz cone (300 μm orifice, 25° opening angle) and transferred into a molecular beam, then directed through a copper skimmer to the ion source of the mass spectrometer. The two-stage Wiley-McLaren ion source with a reflectron time-of-flight (TOF) detection unit provides a mass resolution of $m/\Delta m \sim 4000$, enabling the determination of the exact elemental composition of C/H/O species. Soft ionization energies (10.0, 11.5, 13.0 eV for intermediates, 16 and 18 eV for main species) were used to minimize undesired fragmentation. Ions were detected using a multichannel plate (MCP) with a multichannel scaler for data recording. The mole fraction evaluation followed previously reported procedures [10]. Combined with a gas chromatograph equipped with an Alumina BOND/Na_2SO_4 column, the setup was able to distinguish stable hydrocarbon isomers to provide supplemental information for the evaluation of the EI-MBMS data, which was done using the cross section of the dominant isomer. The same MCP of the EI-MBMS setup was used to detect species of the GC effluent. Generally, in the EI-MBMS experiment the error is <30% for directly calibrated species, and below a factor of 2 for species calibrated with the convolution procedure [10]. For radicals for which the relative ionization cross section (RICS) procedure [11] was used, the error is estimated to be in the range of factors of 2–4. The flame temperature was derived from the pressure in the first pumping stage and calibrated at 20 mm above the burner by OH planar laser-induced fluorescence without the sampling nozzle present [12].

2.3. VUV-PI-MBMS experiment

Information regarding the identification of oxygenated isomers that could not be separated by the present GC setup was obtained using a VUV-PI-MBMS instrument. A detailed description can be found elsewhere [13]. In brief, this system includes modules devoted to sampling and ionization; ion transfer and storage; and ion detection, the latter housing the TOF-MS with a mass resolution of $m/\Delta m \sim 3500$ and a detection limit of <1 ppm. Samples were withdrawn from the flame by a quartz nozzle (400 μm orifice, 25° included angle) to form a molecular beam which was then intersected and ionized by the tunable VUV synchrotron radiation with energy resolution of $E/\Delta E \sim 1000$ and average photon flux of $\sim 10^{12}$ photons/s.

2.4. Flame speed experiments

Laminar flame speeds of DEE were measured in a heated high-pressure, constant-volume cylindrical chamber. Mixtures of DEE/oxygen/nitrogen (4.43%/18.99%/76.58%) at $\phi = 1.4$ were studied with an initial gas temperature of 298 K for pressures of 101, 203, 304, 405, and 507 kPa, respectively. Details of the apparatus and procedures

were described elsewhere [14]. In brief, the cylindrical chamber was housed in an oven and filled with a quiescent combustible mixture and then centrally ignited. The unsteady flame front time history was measured directly using high-speed Schlieren imaging. The time-dependent flame front location data were analyzed by using an automated flame-edge detection and circle-fitting program. The unstretched flame speed relative to the burned gas ($S_{b,0}$) was calculated using the extrapolation procedure described in [14], and this extrapolated flame velocity was converted to the unstretched propagation speed relative to the unburned gas ($S_{u,0}$) using the density ratio calculated by CHEMKIN [15]. The uncertainty of the measured flame speed is below 10%.

2.5. Model development and simulations

A preliminary analysis with the solely available model by Yasunaga et al. [5] showed that the decomposition of the DEE radicals is an essential part of its flame chemistry, hence good kinetic data for these reactions are needed. However, the Yasunaga model was largely constructed using estimated rate constants for the primary reactions. We have therefore used a more accurate quantum chemistry computation method, *i.e.* CBS-QB3, to determine rate constants for several important reaction classes and thermochemical data of related species. Note that while several low-temperature-chemistry studies were reported for the reaction schemes or reaction rate constants of DEE and its radicals [16–18], only very scarce kinetic data is available for the high-temperature oxidation of this fuel.

Thermochemical data for DEE, DEE radicals, and species in the oxidation pathways were obtained from quantum chemistry calculations in the present work or relied on recent results of [19]; these results are provided in Section S.I.1 in Supplemental Material 1. The formation enthalpies for DEE and the $C_2H_5OCHCH_3$ radical calculated in the present work are in good agreement (within 1 kcal/mol) with values in the literature [5,20,21]. A slightly higher discrepancy of 1.54 kcal/mol is noted between the formation enthalpy of the $C_2H_5OCH_2CH_2$ radical from Yasunaga et al. [5] and the value in the present work, which is, however, in good agreement with that in Burcat's database [20].

The new DEE sub-mechanism contains the following major classes of elementary reactions: (i) unimolecular decomposition, (ii) H-atom abstractions, (iii) fuel radical isomerization, (iv) fuel radical decomposition by C–O and C–H bond β-scissions, (v) fuel radical oxidation, (vi) fuel radical–radical disproportionation forming ethyl vinyl ether (EVE, C_4H_8O), and (vii) consumption reactions of primary products. These reaction classes have been thoroughly discussed for several fuels in previous studies [22,23]. Some of these classes, *i.e.* (iii), (vi), and C–H bond β-scissions yielding EVE were not included in the Yasunaga mechanism [5]. Important pathways of DEE combustion are summarized in Fig. 1. Rate constants for C–O and C–H bond β-scissions (channels Ia, Ic, IIa, and IIc in Fig. 1) and isomerization (channel "iso") were calculated here using the CBS-QB3 method; details of the used CBS-QB3 approach are given in [24]. The present model has used high-pressure limiting rate constants for the unimolecular decomposition reactions of the fuel radicals. This is justified by the very low decomposition barriers which are rapidly overcome at the high temperatures of the flame. More information is available in Section S.I. of Supplemental Material 1. The rate constant for C–O bond β-scission of $C_2H_5OCHCH_3$ calculated here is ~700 times slower at 1200 K than that in the Yasunaga model. The DEE radical oxidation by O_2 (Ib, IIb) can lead to the formation of EVE via ethoxyethylperoxy radicals. The role of this reaction class has recently been identified in the low- and high-temperature oxidation of alcohols [23,25]. Rate constants for reactions in these oxidation routes recently calculated by Sakai et al. [19] for the temperature range 500–2500 K are adopted in the present model.

Together with the reactions of the DEE radicals described above, H-abstractions from DEE by H and OH play an important role in DEE combustion. H-abstractions by H-atom have also been investigated here for both α and β positions (see definitions in Fig. 1) to obtain reliable rate constants and branching ratios, while those for H-abstractions by OH are based on theoretical work by Zhou et al. [26]. Note that the Yasunaga model [5] also used the kinetic data from [26], but with an erroneous sign for the activation energy of channel I (4040 cal/mol instead of –4040 cal/mol). Rate constants of H-abstractions by H-atom calculated here are about two times slower at 1200 K than those in the Yasunaga model [5]. Additional information on the thermochemical data and rate constants calculated in the present work is available in Supplemental Material 1.

Pressure-dependent rate constants for the unimolecular decompositions of DEE were taken from Yasunaga et al. [5]. Missing C–H bond scissions were added with estimated rate constants of 1×10^{14} cm^3/mol s for the recombination of H-atoms with the DEE radicals. The DEE sub-mechanism has been added to the recently updated NUIG database [27] without any changes to ensure internal consistency. Reactions of most of the primary products (ethylene, acetaldehyde, ethanol, formaldehyde, etc.) are already included in the reaction base and decomposition reactions of ethyl vinyl ether have been taken from [24]. Reactions of some products involved in low-temperature oxidation were newly added, and high-pressure limiting rate constants were used for unimolecular initiation

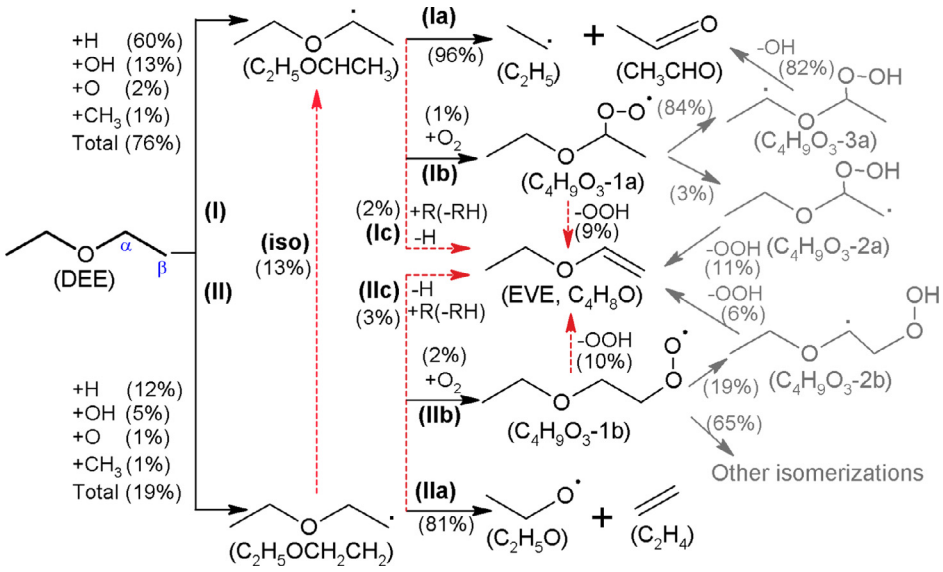

Fig. 1. Important DEE reaction pathways. Percentages given are relative rates of consumption of a species in the present low-pressure flame, analyzed in the region of 0–100% fuel conversion. Pathways indicated by dashed lines were not considered in the Yasunaga model [5].

reactions. However, previous work [24] demonstrated that the latter reaction class has minor importance under premixed flame conditions. Moreover, successions of H-abstractions/β-scissions of low-temperature oxidation products were written as irreversible since the reverse rate constants cannot be calculated from the global equilibrium constants. Transport properties of species for which no data is available in the literature were estimated based on the correlations proposed by Wang and Frenklach [28]. The complete reaction mechanism for DEE combustion includes 2385 elementary reactions among 380 chemical species and is available in CHEMKIN format together with thermodynamic and transport properties in Supplemental Material 2.

Prior to applying the newly developed kinetic model to simulate the current experimental data, it was tested against several datasets published in the literature, measured in non-premixed flames [6], pyrolysis experiments [5], and including ignition delay times [4,5] and flame speeds [7], with encouraging results (see Supplemental Material 1, Section S.I.2.). Simulations were performed using CHEMKIN [15] for premixed flames and OpenSMOKE++ [29] for other configurations.

3. Results and discussion

3.1. Species profiles in premixed low-pressure flame

In this study, more than 40 species, including reactants, products, stable intermediates, and radical species, were identified and quantified. Temperature and mole fraction profiles of the main species (DEE, O_2, Ar, CO, CO_2, H_2O, and H_2) as a function of the distance above the burner (h) as well as species mole fractions with the respective calibration method, electron energy, and literature ionization threshold for each intermediate are available in Supplemental Material 1, Fig. S12 and Table S4. Isomer identification is provided in Section S.II.2. Fig. S12 shows that DEE is fully consumed at $h > 3.5$ mm. The mole fractions of the main species at $h = 30$ mm are close to equilibrium values.

In the following, we discuss selected intermediate species, with a special focus on primary species, defined as those produced directly from the fuel or from its radicals. The discussion includes the comparison of experiments and predictions by the present kinetic model and that of Yasunaga et al. [5] and analyzes the degradation pathways of DEE together with the formation of intermediates. Figs. 2–4 display mole fraction profiles of selected labile and stable intermediates in the range of C_1–C_6. Overall, they show reasonable agreement, especially with respect to the peak locations and profile shapes, between experiment and predictions by both models. Note that the present model predicts also well the pyrolysis and ignition delay time data of Yasunaga et al. [5] as mentioned earlier.

The performance of the present model can be further analyzed regarding the degradation pathways of DEE. Fig. 1 includes a rate-of-production (ROP) analysis with this model for DEE consumption, globally performed in the region of 0–100% fuel conversion. Under these conditions, H-abstraction reactions are responsible for ~95% of

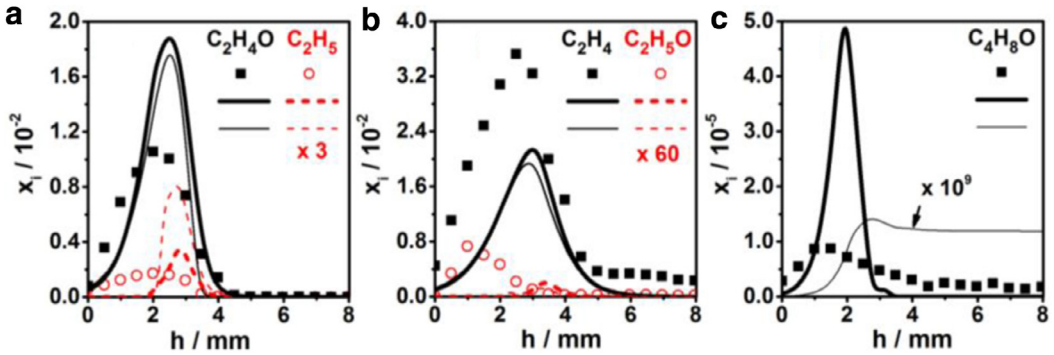

Fig. 2. Mole fraction profiles of "direct" primary species: C_2H_5, C_2H_4O, C_2H_4, C_2H_5O, C_4H_8O. Symbols: experiment, thick lines: present model, thin lines: Yasunaga model [5]. For clarity, the indicated multiplication factors have been used (for experiments and both models) for C_2H_5 and C_2H_5O.

total DEE consumption. H-abstractions by flame-propagating radicals mainly (~76%) occur at the $C_{-\alpha}$ position of DEE (see Fig. 1) because of its lowest C–H bond energy (96 kcal/mol), yielding the $C_2H_5OCHCH_3$ radical. H-abstractions from the $C_{-\beta}$ positions (C–H bond energy of 103 kcal/mol) producing the $C_2H_5OCH_2CH_2$ radical account for ~19% of total DEE consumption. Both fuel radicals, *i.e.* $C_2H_5OCHCH_3$ and $C_2H_5OCH_2CH_2$, react largely by C–O bond β-scission leading to the formation of acetaldehyde (CH_3CHO) + ethyl (C_2H_5) and ethylene (C_2H_4) + ethoxy (C_2H_5O), respectively. Another fraction of these two fuel radicals is consumed by oxidation, disproportionation, and C–H bond β-scissions producing EVE, which is consumed by H-abstraction and retro-ene reactions. Note that the four-centered elimination DEE(+M)→C_2H_5OH+C_2H_4(+M) (not shown in Fig. 1) plays only a minor role (<2%) in DEE consumption in the present low-pressure flame.

Species produced directly from the two DEE radicals via β-scissions (here called "direct" primary intermediates) are presented in Fig. 2. C_2H_4O and C_2H_4 were measured with very high mole fractions of 1.05×10^{-2} and 3.53×10^{-2}, respectively. By VUV-PI-MBMS, C_2H_4O was identified as acetaldehyde (~95%) and vinyl alcohol (~5%), see Fig. S14. C_4H_8O (Fig. 2c) was evaluated as EVE and is present at lower concentration than C_2H_4O and C_2H_4. It is important to note that the photoionization efficiency (PIE) spectra of $m/z = 72$ from VUV-PI-MBMS show a clear onset near the IP of EVE (8.98 eV [21], see Fig. S14). Although the formation of EVE accounts for only ~5% of the consumption of the fuel radicals, this intermediate species is important because it is a primary fuel destruction product that was unambiguously identified for the first time in DEE combustion. C_2H_5 and C_2H_5O were detected at much lower concentrations (see Fig. 2) because of their high reactivity. However, their subsequent reactions contribute significantly to the formation of further important intermediates. C_2H_5 reacts with H to produce CH_3 that in turn reacts with H or HCO, contributing with ~55% to the formation of CH_4. The latter species was measured with a high mole fraction of 1.9×10^{-2}. Other reactions of C_2H_5 partially contribute to the formation of C_2H_4 (by C–H bond β-scission, oxidation, or disproportionation), C_2H_6 (by recombining with H-atom), C_3H_8 (by recombining with CH_3), and C_4H_{10} (by self-recombination). These species, which are presented in Fig. 3, are overall reasonably predicted by the present model. C_4H_{10} was identified by GC to be exclusively *n*-butane. C_2H_5O in turn decomposes mainly into formaldehyde (CH_2O) and CH_3 by C–O bond β-scission. The C_2H_5O radical also recombines with an H-atom to produce ethanol (C_2H_6O). Under the present flame conditions, these two pathways contribute significantly to the formation of formaldehyde (~60%) and ethanol (20%), respectively. Formaldehyde was detected with a high mole fraction of 1.2×10^{-2} (see Fig. 3e).

The mole fractions of several other C_1–C_6 products including radical and stable species are presented in Fig. 4. These species are produced mainly by secondary reactions, as supported by the ROP analysis from the kinetic model. The corresponding reactions are part of the base mechanism and not the focus of this work. Since acetaldehyde is a dominant primary species of DEE combustion, its decomposition contributes to the formation of several species, detected in the present flame, as discussed hereafter. Methanol (CH_4O) with a measured mole fraction of 7.9×10^{-4} (Fig. 4a) is mainly produced by the disproportionation reaction of two CH_3O, and by H-abstractions from acetaldehyde by CH_3O. The profile of C_3H_6O is also shown in Fig. 4a as a sum of propanal and acetone; both isomers were identified by VUV-PI-MBMS.

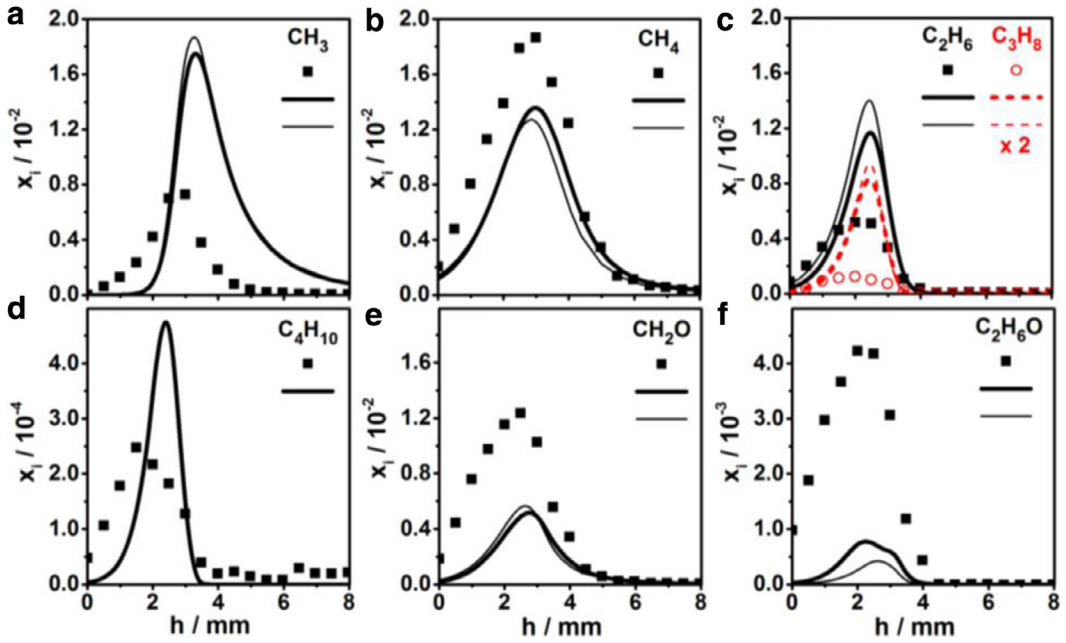

Fig. 3. Mole fraction profiles of further important species: CH_3, CH_4, C_2H_6, C_3H_8, C_4H_{10}, CH_2O, C_2H_6O. Symbols: experiment, thick lines: present model, thin lines: Yasunaga model [5]. For clarity, a multiplication factor of 2 has been used (for experiments and both models) for C_3H_8.

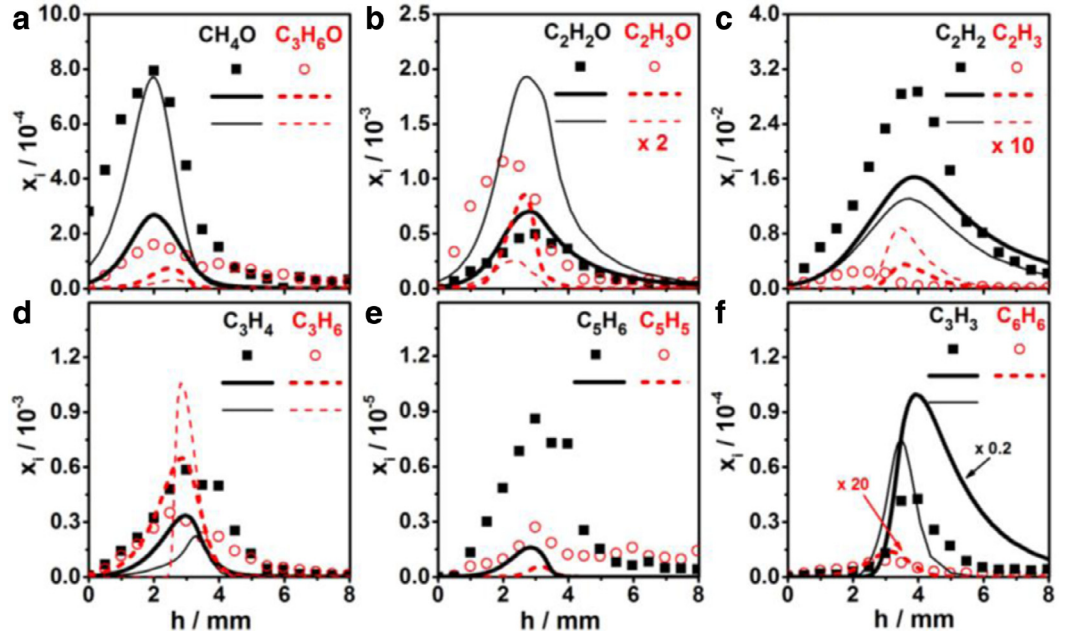

Fig. 4. Mole fraction profiles of other labile and stable intermediates in the C_1–C_6 range. Symbols: experiment, thick lines: present model, thin lines: Yasunaga model [5]. For clarity, the indicated multiplication factors have been used (for experiments and both models) for some species, with the exception of C_3H_3 and C_6H_6 for which only the simulation with the present model was multiplied by 0.2 and 20 respectively.

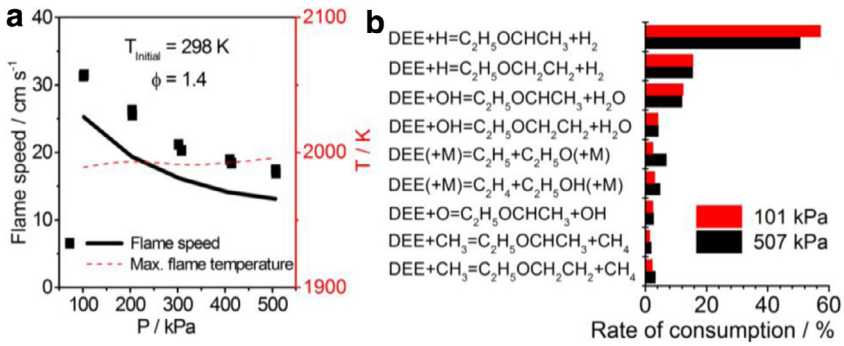

Fig. 5. (a) Flame speeds of DEE and related maximum flame temperature. Symbols: experiment, lines: present model. (b) Relative consumption rates of DEE at 101 and 507 kPa.

According to the model, the formation of propanal and acetone mainly results from combination of CH_3 with the acetaldehyde radicals CH_2CHO and CH_3CO (*i.e.* $CH_3+CH_2CHO⇆C_2H_5CHO$, $CH_3+CH_3CO⇆C_2H_6CO$). The profile for the sum of these acetaldehyde radicals (C_2H_3O) is presented in Fig. 4b, together with that for ketene (C_2H_2O) which is produced mainly from $CH_3CO+CH_3⇆C_2H_2O+CH_4$. The prediction for ketene is clearly better in the present model. Small C_2–C_6 soot precursors are also presented in Fig. 4. C_5H_6 (1,3-cylopentadiene), C_5H_5 (cylopentadienyl radical), and C_6H_6 (benzene), known as important cyclic soot precursors, were detected at low mole fractions ($<10^{-5}$), while smaller species including C_2H_2 (Fig. 4c), C_3H_4, and C_3H_6 (Fig. 4d) are present in the 10^{-2}–10^{-4} range. According to the GC analysis, allene and propyne are identified for C_3H_4 isomers with propyne as the most abundant one. C_4H_6 is for a large part 1,3-butadiene, and C_4H_8 is predominantly 1-butene. The present model also predicts these trends (see Table S5), while the Yasunaga model [5] does not include reactions for the formation of hydrocarbon species from C_4. Fig. 4f shows the peak location of C_6H_6 to be closer to the burner than that of C_3H_3 (propargyl). Although an under-prediction is noted for benzene, the model represents this trend in peak locations, indicating that the main route of benzene formation is likely not propargyl recombination. Benzene is predicted to be largely produced by the recombination of an H-atom and the C_6H_5 radical or C_3H_3 and C_3H_5 radicals. Because of its very low mole fraction ($<10^{-5}$), benzene was difficult to be well predicted by the present model (under-prediction by a factor of ~20), however, with higher concentrations, *e.g.* in sooting flames, its prediction could be expected to be improved.

3.2. Flame speeds at elevated pressure

To study the DEE high-temperature reaction chemistry at elevated pressures, flame speeds of DEE were measured at an initial temperature of 298 K for $\phi \sim 1.4$ at pressures of 101, 203, 304, 405, and 507 kPa. The results are presented in Fig. 5a along with predictions by the present kinetic model. The flame speed decreases with increasing pressure, a trend well captured by the present model which, however, under-predicts the absolute flame speeds by ~16%. The predicted flame temperature rises only slightly with increasing pressure. Sensitivity analyses (not shown) indicate that the kinetics of small species control the flame speed at all studied conditions. The chain-branching reaction of O_2 with H, producing OH and O ($O_2+H⇆OH+O$) promotes the reactivity significantly, while the three-body termination reaction $H+CH_3(+M)⇆CH_4(+M)$ has the largest effect on the reduction of flame propagation, especially at high pressures, since this reaction reduces the H-atom concentration and competes with the former. No large sensitivity was seen for the primary reactions involving DEE decomposition and oxidation. Hence, the observed deviations between model and experiment could result from uncertainties in the small-species kinetics in the base mechanism and/or in the experiment. Note that the present model well predicts the flame speed data by Gillespie et al. [7] (Fig. S11). Different uncertainties of the two setups and different sensitivities of the model under the two different inlet conditions could contribute to the noted discrepancies.

The ROP analysis in Fig. 5b indicates that a large part of DEE is consumed by H-abstractions by flame-propagating radicals, especially with H and OH. This trend is similar to that observed in the low-pressure flame described earlier. Note that the contribution of the four-centered elimination $DEE(+M)→C_2H_4+C_2H_5OH(+M)$ and the C–O bond scission $DEE(+M)→C_2H_5+C_2H_5O(+M)$ to the DEE consumption increases with increasing pressure, suggesting that the distribution of ethanol and acetaldehyde will change with pressure.

4. Summary

The high-temperature combustion chemistry of DEE was investigated experimentally with a focus on obtaining quantitative species profiles at flame conditions. More than 40 species were identified and quantified in a low-pressure fuel-rich ($\phi \sim 1.8$) premixed flame using EI-MBMS-GC, complemented with VUV-PI-MBMS. The data provides a good basis for model development and examination. Furthermore, high-pressure flame speeds of DEE were determined at an initial gas temperature of 298 K, at $\phi = 1.4$, from 101 to 507 kPa. The obtained experimental results were compared to predictions with a newly developed detailed kinetic model that contains systematically updated thermochemical and kinetic data from dedicated CBS-QB3 calculations. Reasonable agreement between experiment and predictions by the proposed mechanism was observed. Acetaldehyde, known as carcinogen for humans, was detected at high amounts, in agreement with the model prediction. It is seen to be largely produced from the dominant pathway of DEE consumption via H-abstractions followed by β-scissions. However, cyclopentadiene and benzene, known as important soot precursors, were measured at low mole fractions ($<10^{-5}$). The DEE flame speed was observed to decrease with increasing pressure, and it is affected strongly by the kinetic of small species. The present study demonstrates that at all pressures investigated, DEE consumption is mainly controlled by H-abstractions by H and OH and subsequent decomposition of the fuel radicals. Theoretical calculations were used in particular to determine reliable rate constants and branching ratios for these reactions. Among the unimolecular pathways, only the four-centered elimination and the C–O bond scission contributed to a minor degree to DEE consumption, and this contribution increases with pressure.

Acknowledgments

L.S.T. thanks the Alexander von Humboldt Foundation for a research fellowship. The authors thank their colleagues Y. Li, B. Yang, and their students for discussions and for their help and contribution to some PIE spectra using the PI-MBMS setup at National Synchrotron Radiation Research Center. Also we thank M. Zeng for participation in some of the simulations. Y.J. would like to thank the grant support of NSF CBET-1507358.

Supplementary materials

Supplementary material associated with this article can be found, in the online version, at doi:10.1016/j.proci.2016.06.087.

References

[1] K. Kohse-Höinghaus, P. Oßwald, T.A. Cool, T. Kasper, N. Hansen, F. Qi, C.K. Westbrook, P.R. Westmoreland, Angew. Chem. Int. Ed. 49 (21) (2010) 3572–3597.
[2] A. Paul, P.K. Bose, R. Panua, D. Debroy, J. Energy Inst. 88 (1) (2015) 1–10.
[3] D.C. Rakopoulos, C.D. Rakopoulos, E.G. Giakoumis, A.M. Dimaratos, *Energy* 43 (1) (2012) 214–224.
[4] M. Werler, L.R. Cancino, R. Schiessl, U. Maas, C. Schulz, M. Fikri, *Proc. Combust. Inst.* 35 (2015) 259–266.
[5] K. Yasunaga, F. Gillespie, J.M. Simmie, H.J. Curran, Y. Kuraguchi, H. Hoshikawa, M. Yamane, Y. Hidaka, *J. Phys. Chem. A* 114 (34) (2010) 9098–9109.
[6] J. Hashimoto, K. Tanoue, N. Taide, Y. Nouno, *Proc. Combust. Inst.* 35 (2015) 973–980.
[7] F. Gillespie, W.K. Metcalfe, P. Dirrenberger, O. Herbinet, P.-A. Glaude, F. Battin-Leclerc, H.J. Curran, *Energy* 43 (1) (2012) 140–145.
[8] Y. Di, Z. Huang, N. Zhang, B. Zheng, X. Wu, Z. Zhang, *Energy Fuels* 23 (5) (2009) 2490–2497.
[9] N. Zhang, Y. Di, Z. Huang, B. Zheng, Z. Zhang, *Energy Fuels* 23 (12) (2009) 5798–5805.
[10] M. Schenk, L. Leon, K. Moshammer, P. Oßwald, T. Zeuch, L. Seidel, F. Mauss, K. Kohse-Höinghaus, *Combust. Flame* 160 (3) (2013) 487–503.
[11] J.C. Biordi, *Prog. Energy Combust. Sci.* 3 (3) (1977) 151–173.
[12] X. Yang, D. Felsmann, N. Kurimoto, J. Krüger, T. Wada, T. Tan, E.A. Carter, K. Kohse-Höinghaus, Y. Ju, *Proc. Combust. Inst.* 35 (2015) 491–498.
[13] Z.Y. Zhou, Y. Wang, X.F. Tang, W.H. Wu, F. Qi, *Rev. Sci. Instrum.* 84 (1) (2013) 014101.
[14] D. Liu, J. Santner, C. Togbe, D. Felsmann, J. Koppmann, A. Lackner, X. Yang, X. Shen, Y. Ju, K. Kohse-Höinghaus, *Combust. Flame* 160 (12) (2013) 2654–2668.
[15] CHEMKIN-PRO 15092, *Reaction Design* (2009).
[16] R.S. Tranter, R.W. Walker, *Phys. Chem. Chem. Phys.* 3 (21) (2001) 4722–4732.
[17] S. Di Tommaso, P. Rotureau, O. Crescenzi, C. Adamo, *Phys. Chem. Chem. Phys.* 13 (32) (2011) 14636–14645.
[18] J. Zádor, C.A. Taatjes, R.X. Fernandes, *Prog. Energy Combust. Sci.* 37 (4) (2011) 371–421.
[19] Y. Sakai, H. Ando, H.K. Chakravarty, H. Pitsch, R.X. Fernandes, *Proc. Combust. Inst.* 35 (2015) 161–169.
[20] E. Goos, A. Burcat, B. Ruscic, available at <http://burcat.technion.ac.il/dir/>.
[21] NIST Chemistry WebBook, available at < http://webbook.nist.gov/chemistry/>.
[22] H.J. Curran, P. Gaffuri, W.J. Pitz, C.K. Westbrook, *Combust. Flame* 114 (1–2) (1998) 149–177.
[23] S.M. Sarathy, S. Vranckx, K. Yasunaga, M. Mehl, P. Oßwald, W.K. Metcalfe, C.K. Westbrook, W.J. Pitz, K. Kohse-Höinghaus, R.X. Fernandes, H.J. Curran, *Combust. Flame* 159 (6) (2012) 2028–2055.
[24] L.-S. Tran, R. De Bruycker, H.-H. Carstensen, P.-A. Glaude, F. Monge, M.U. Alzueta, R.C. Martin, F. Battin-Leclerc, K.M. Van Geem, G.B. Marin, *Combust. Flame* 162 (11) (2015) 4283–4303.

[25] G. da Silva, J.W. Bozzelli, L. Liang, J.T. Farrell, *J. Phys. Chem. A* 113 (31) (2009) 8923–8933.
[26] C.-W. Zhou, J.M. Simmie, H.J. Curran, *Phys. Chem. Chem. Phys.* 12 (26) (2010) 7221–7233.
[27] S.M. Burke, W. Metcalfe, O. Herbinet, F. Battin-Leclerc, F.M. Haas, J. Santner, F.L. Dryer, H.J. Curran, *Combust. Flame* 161 (11) (2014) 2765–2784.
[28] H. Wang, M. Frenklach, *Combust. Flame* 96 (1-2) (1994) 163–170.
[29] A. Cuoci, A. Frassoldati, T. Faravelli, E. Ranzi, *Comput. Phys. Commun.* 192 (2015) 237–264.